化 学 学 报
ACTA CHIMICA SINICA

研究论文
Article

DOI: 10.6023/A13030253

$C_{12}EO_4$ 与氨丙基三乙氧基硅烷水溶液自组装和流变性研究

郭红　王栋　董姝丽　窦盈莹　宋爱新　郝京诚*

(山东大学胶体与界面化学教育部重点实验室　济南 250100)

摘要　研究了 3-氨丙基三乙氧基硅烷(APTES)和非离子表面活性剂十二烷基聚氧乙烯($C_{12}EO_4$)水溶液的相行为、溶液自聚集作用和流变性, 小角度 X-射线散射(SAXS)、低温透射电子显微镜(cryo-TEM)和氘谱核磁共振(^{2}H NMR)测定确定了溶液中聚集体结构, 测定了聚集体混合物溶液的流变性质. 结果表明: 随着溶液混合物组分的变化, 溶液聚集体结构发生了改变, 在 L_α 相区内, 恒定 $C_{12}EO_4$ 浓度, 随着 APTES 浓度增加聚集体结构由高曲率聚集体转变为低曲率的层状结构; 而在恒定 APTES 浓度时, 随着 $C_{12}EO_4$ 增加, L_α 相由低粘弹性的囊泡溶液转变为粘弹性极高的密堆积囊泡和平面层状结构共存的类凝胶相, 溶液聚集体结构和结构转变是由于 APTES 水解产物插入至 $C_{12}EO_4$ 胶束引起的. 非离子表面活性剂和氨基硅烷混合物溶液相结构及结构转变的新结果对于完全理解该类混合物的实际应用, 特别是作为模板合成硅材料的应用具有重要理论意义.

关键词　相行为; 非离子表面活性剂; 氨基硅氧烷; 流变性; cryo-TEM

Self-assembly and Rheological Properties of $C_{12}EO_4$ and Aminosilane Mixtures

Guo, Hong　Wang, Dong　Dong, Shuli　Dou, Yingying
Song, Aixin　Hao, Jingcheng*

(*Key Laboratory for Colloid and Interface Chemistry* (*Shandong University*), *Ministry of Education*, *Jinan 250100*)

Abstract　Phase behavior, self-assembly, and rheological properties of 3-aminopropyltriethoxysilane (APTES) and nonionic surfactant, $CH_3(CH_2)_{11}(OCH_2CH_2)_4OH$ ($C_{12}EO_4$), in water were studied. The self-assembled structures were determined by means of small angle X-ray scattering (SAXS), cryo-transmission electron microscopy (cryo-TEM), freeze-fracture TEM (FF-TEM), and ^{2}H nuclear magnetic resonance (^{2}H NMR) measurements and the properties of self-assembled mixtures were obtained by rheological measurements. With a variation of the composition, different self-assembled structures were obtained. In the L_α phase region, a phase structural transition from an aggregate with high curvatures to the lamellar structures with low curvatures is observed with an increase of APTES concentration at a constant concentration of $C_{12}EO_4$. At constant APTES concentration, with an increase of $C_{12}EO_4$ concentration, densely packed vesicles and planarly lamellar structures which behave the properties as gel-like solutions having the rather high viscosity coexist. The phase structural transition was considered to be induced by the insertion of the hydrolytic products of APTES into the palisade of the micelles of $C_{12}EO_4$. These new observations on phase structural transition and self-assembly of nonionic surfactant and aminosilane mixtures could be very important for the full understanding for their applications, especially as templates in the synthesis of silica materials, *etc*.

Keywords　phase behavior; nonionic surfactant; aminosilane; rheological property; cryo-TEM

1　Introduction

The phase behavior of poly(oxyethylene) monoalkyl ether nonionic surfactants, $CH_3(CH_2)_{n-1}(OCH_2CH_2)_mOH$ (abbreviated as C_nEO_m), in aqueous solution has aroused great interests in recent years.[1] The self-assembly was widely used in the solubilization of substances,[2] material synthesis,[3,4] cosmetic products, and industrial processes, *etc*. Extensive research on the effect of the alkyl length and the size of headgroup on phase behavior and self-assembly were carried out in the past few decades.[5,6] Particular attention was paid to the combination of C_nEO_m with other surfactants such as cationic and anionic surfactants.

C_nEO_m family exhibits rich phase behavior in aqueous solutions and are widely used in the synthesis of mesoporous silica.[3,7] For various polyoxyethlene surfactants, various phases like spherical micelles (I_1), hexagonal liquid crystallines (H_1), normally bicontinuous phases (V_1), lamellar phases (L_α), and reversed bicontinuous phases (V_2) were observed. It was found that large headgroups and low temperature favor the formation of aggregates with high curvature such as I_1 and H_1 phases, while surfactant molecules with small headgroups tend to form L_α and reverse phases, and the increase of EO number is unfavorable for forming L_α phase.[8]

For the study of anionic/nonionic surfactant mix-

* E-mail: jhao@sdu.edu.cn; Tel.: 0531-88366074; Fax: 0531-88564750
Received March 7, 2013; published May 16, 2013.
Project supported by the National Natural Science Foundation of China (Nos. 21033005, 21273136) and the National Basic Research Program of China (973 Program, No. 2009CB930103).
项目受国家自然科学基金(Nos. 21033005, 21273136)和国家重大研究计划(973 计划, No. 2009CB930103)资助.

tures,[9,10] most attention has been focused on the self-assembly and phase behavior for C_nEO_m and sodium dodecyl sulfate (SDS) system.[1] Upon the addition of $C_{12}EO_n$ with short EO group (n=2, 3, 4) to dilute SDS solution, the one-dimensional growth of micelles in SDS and $C_{12}EO_n$ aqueous mixtures can be observed and the highly viscoelastic wormlike micelles appear above a certain concentration; moreover, the addition of $C_{12}EO_3$ to SDS solution induced the faster micellar growth than that of $C_{12}EO_4$.[6] With an increase of $C_{12}EO_4$ amount, the wormlike micelles evolve continuously to be followed as entanglement, rodlike, and branching micelles.[11] Recently, we reported the interaction of $C_{12}EO_4$ with a commercially anionic surfactant, sodium bis(2-ethyl hexyl) sulfosuccinate (AOT), and discovered the formation of onion-like vesicles with the addition of AOT to $C_{12}EO_4$ solutions, demonstrating the existence of an attractive interaction between the two surfactants.[12]

3-Aminopropyltriethoxysilane (APTES) is one kind of functional trialkoxysilanes which is extensively used as cross-linkers, adhesion promoting primers, coupling agents, and surface modification agents.[13,14] In aqueous solution, APTES shows a pronounced tendency for hydrolysis via a series of consecutive pseudo first-order reactions presented as follows:[15]

$$\text{R-Si(OR')}_3 \xrightarrow{k_1} \text{R-Si(OR')}_2\text{OH} \xrightarrow{k_2} \text{R-(OR')(OH)}_2$$

$$\xrightarrow{k_3} \text{R-Si(OH)}_3$$

where k_1, k_2 and k_3 represent the pseudo first-order reaction rate constant, respectively. These hydrolysis reactions are followed by silanepolyol condensation, which has been demonstrated by FT-IR spectra.[16]

APTES is widely used in the modification of silica surface. In recent years, many results about the synthesis of silica materials by using nonionic surfactant aggregates as templates were reported.[3,7] However, the aggregation behavior and the self-assembly induced by APTES were rarely reported, which is a deficiency for the detection of the mechanism. In the present work, we studied the phase behavior, self-assembly, and the phase structural transition of the microstructures of $C_{12}EO_4$ and APTES mixtures with varying the compositions in aqueous solutions. We hope that the study on aggregation behavior and self-assembly may provide the guidance as templates of nonionic surfactants and aminosilanes mixtures in the synthesis of silica materials.

2 Experimental

2.1 Chemicals

$C_{12}EO_4$ was purchased from Acros Organics (USA) (>99%). 3-Aminopropyltriethoxysilane (APTES, >98%) was purchased from J&K Chemicals (Beijing, China). D_2O (≥99.9%) was purchased from Aldrich. All of the chemicals were directly used without further purification. Ultrapure water with a resistivity of 18.25 MΩ•cm was obtained using a UPH-IV ultrapure water purifier (China).

2.2 Method and characterization

Required amounts of APTES, $C_{12}EO_4$, and water were added into clean vials and sealed to avoid water evaporation. The samples were mixed with a vortex mixer and ultra-sonicated at 45 ℃ for 3 h in a bath ultrasonic apparatus to make the samples be dispersed sufficiently. Then the samples were equilibrated at 25.0±0.1 ℃ for at least 4 weeks before the phase behavior was inspected. The phase diagram was drawn on the basis of visual inspection with the help of crossed polarizers.

The rheological measurements were carried out on a HAAKE RS6000 rheometer with a cone-plate system (Ti, diameter, 35 mm; cone angle, 1°). In oscillatory measurements, an amplitude sweep at a fixed frequency of 1 Hz was performed prior to the following frequency sweep in order to ensure that the selected stress was in the linear viscoelastic region. The viscoelastic properties of the samples were determined by oscillatory measurements in the frequency range of 0.01 to 10 Hz. The samples were measured at 25.0±0.1 ℃ with the help of a cyclic water bath.

Samples for ^{2}H NMR measurements were prepared in D_2O. ^{2}H NMR spectra were carried out on a Bruker Avance 400 spectrometer equipped with a pulse field gradient module (z-axis). All experiments were operated at 25.0±0.1 ℃.

SAXS experiments were performed at Beamline 4B9A at Beijing Synchrotron Radiation Facility at 25 ℃. The imaging plate was a Mar165 with a resolution factor of 2048×2048. The two-dimensional SAXS scattering patterns were composed of concentric circles, and the intensity (I) versus scattering vector (q) profile was independent of the azimuthal angle. The range of scattering vectors was chosen from 0.05 to 4 nm^{-1} (q=[4π•sin(θ/2)]/λ, where θ and λ are the scattering angle and the incident X-ray wavelength, respectively). The distance from the sample to the detector was 1610 mm, and the data accumulation time was 300 s for each sample.

For cryo-TEM observations, about 5 μL of solution was loaded onto a TEM grid, and the redundant liquid solution was removed with two pieces of filter paper, leaving a thin film suspended on the mesh holes. The samples were rapidly dipped into a reservoir which was filled with liquid ethane cooled by liquid nitrogen, resulting in the vitrification of the samples. Then the vitrified samples were plunged into liquid nitrogen until they were transferred to a cryogenic sample holder (Gatan 626). The observations of the samples were carried out with a JEOL JEM-1400 TEM (120 kV) at about −174 ℃. The images were recorded on a Gatan multiscan CCD and processed with Digital Micrograph.

For FF-TEM determination, a small drop of solution, *ca.* 4 μL was loaded on a specimen holder and was quickly frozen by plunging the specimen holder into liquid ethane which was cooled by liquid nitrogen. Fracturing and replication were carried out on a freeze-fracture apparatus (Leica EM BAF 060, Germany) at −150 ℃. Pt/C was deposited at an angle of 45° to form the replica and C was deposited at an angle of 90° to consolidate the replica. The replica was transferred onto copper grid and observed with a JEOL JEM-1400 TEM at 120 kV.

3 Results and discussion

3.1 Phase behavior

In order to obtain the phase behavior, about 200 samples were prepared. The partial phase diagram of $C_{12}EO_4$/APTES/H_2O system at 25 ℃ is shown in Figure 1. It is well-known that a planar lamellar phase is observed in the wide range of concentration in $C_{12}EO_4$/H_2O system.[17,18] With an variation of the composition, rich phase behavior can be observed. At low and high $C_{12}EO_4$ concentrations, *i.e.*, within the region at lower than 20 wt% and higher than 30 wt%, with the addition of APTES, the slightly turbid L_α phase turns to a L_1/L_α two-phase with a homogeneous L_1 phase equilibrating with a slightly turbid L_α. With the further addition of APTES, two coexisting micellar phases (L_1/L_1'-phase) and finally a transparent L_1-phase appear. When $C_{12}EO_4$ concentration is in the middle region, between about 10 wt% and 45 wt%, a three-phase region appears between the L_1 phase and L_α phase. Within the L_α-phase region, with a variation of the composition, a phase structural transition between vesicles and planar lamellae was detected.

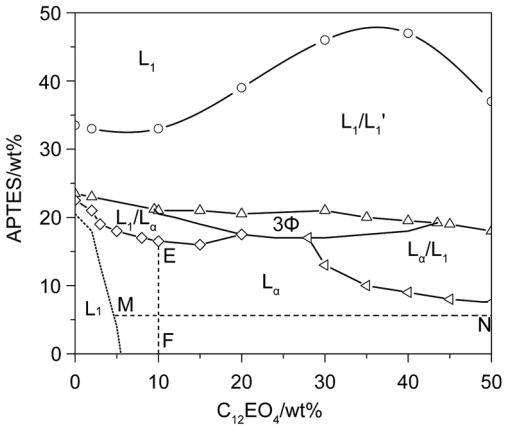

Figure 1 Phase diagram of $C_{12}EO_4$/APTES/H_2O system at 25 ℃. The dotted border represents that the boundary between L_1 and L_α phase region is difficult to be determined.

For the further study on the phase behavior, two series of samples were selected, as shown in lines "EF" and "MN" in Figure 1. For the line "EF", different amounts of APTES were dissolved in 10 wt% $C_{12}EO_4$ solution, and for line "MN", the APTES concentration is fixed to 5 wt%, while the $C_{12}EO_4$ concentration is changeable. Figure 2 shows the phase transition process along line "EF". For the L_α phase of 10 wt% $C_{12}EO_4$, the solution displays slight birefringence. With an increase of APTES concentration, the birefringence becomes obvious and a bright texture appears when APTES reaches 15 wt%. When the APTES concentration continues to increase, the birefringent L_α phase is gradually replaced by the transparent solutions. The macroscopic change indicates the variation of the microstructure.

3.2 ^{2}H NMR and microstructure detection

The ^{2}H NMR experiments are useful and convenient for determining the anisotropy of different phases in surfactant solutions.[19~22] When ^{2}H nucleus is put in an external magnetic field, the spectrum of ^{2}H NMR depends on the interaction between the deuteron quadrupole moment and the electric field gradients around the nucleus.[23,24] For isotropic system, as D_2O molecules experience a macroscopically isotropic environment such as micelle or cubic phase, a single peak appears in the spectra. When D_2O molecules are located in a macroscopically anisotropic environment such as a planar lamellar phase or a hexagonal phase, the quadrupole interaction exists a non-zero average, resulting in a splitting of the resonance due to the anisotropic rotation of D_2O molecules.[23,25~27] Thus, a broad single peak is usually obtained in vesicle phase, while a doublet quadrupole splitting is characterized in long-ranged macroscopically anisotropic planar lamellar phase. When the lamellar phase is arranged orderly, one can observe the simple double peaks under the interaction of magnetic field. While for the lamellar phase outstretched in unordered structure, the spectra are diverse and sometimes exhibit peaks like powder pattern.[23]

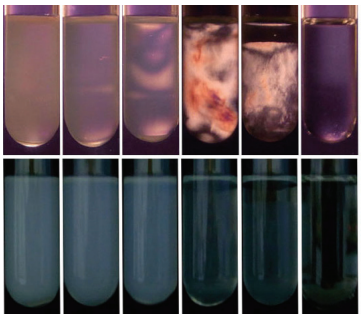

Figure 2 Photographs of samples of 10 wt% $C_{12}EO_4$ and different mass fraction of APTES, from left to right: 0, 5, 10, 15, 20, and 40 wt%, respectively. The photographs were taken with (top) and without (bottom) crossed polarizers.

Figure 3 shows the ^{2}H NMR spectra of four selected samples along the Line "EF" in Figure 1 formed by 10 wt% $C_{12}EO_4$ and different APTES concentrations. One can see that a broad single peak appears in the spectrum of 10 wt% $C_{12}EO_4$ solution, which is due to the average signals of the unordered lamellae at low concentration. With an increase of APTES concentration, the single peak transforms to a splitting double peak gradually, indicating a transition process from unordered structures to ordered lamellar structure, which facilitates the extent of the anisotropy of the environment. The transition can also be reflected by cryo-TEM images, as shown in Figure 4. For the sample of 10 wt% $C_{12}EO_4$/12.5 wt% APTES, the onion-like multi-lamellar vesicles can be observed in Figure 4a, which is in correspondence with ^{2}H NMR spectrum in Figure 3c. At higher APTES concentration, for the sample of 10 wt% $C_{12}EO_4$/17 wt% APTES, the lamellar structures become more planar with low curvature (Figure 4b), inducing the macroscopically anisotropic environment for D_2O to locate, which is in consistence with ^{2}H NMR in Figure 3d.

The ^{2}H NMR spectra of samples along the Line "MN" in Figure 1 formed by 5 wt% APTES and different $C_{12}EO_4$ concentrations are shown in Figure 5. With an increase of $C_{12}EO_4$ concentration, the single sharp peak of 5 wt% APTES/10 wt% $C_{12}EO_4$ exhibits an abundant transition process. When $C_{12}EO_4$ concentration reaches 30 wt%, the

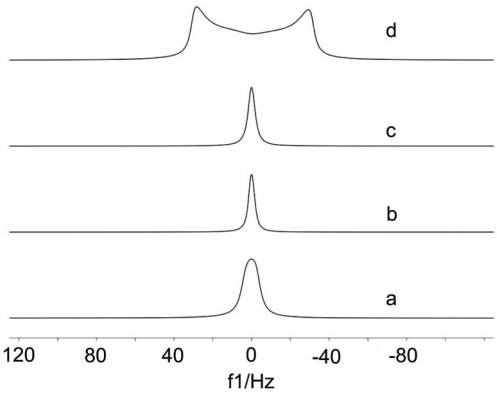

Figure 3 ^{2}H NMR spectra of samples formed by 10 wt% $C_{12}EO_4$ with 0 (a), 7.5 (b), 12.5 (c), and 17 wt% APTES (d) at 25 ℃.

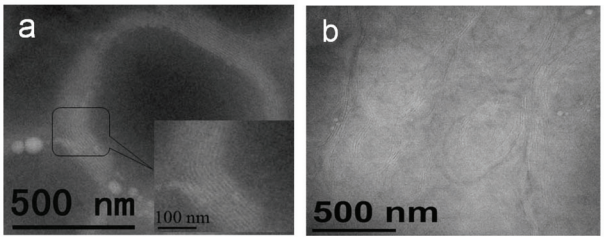

Figure 4 Cryo-TEM images of samples formed by 10 wt% $C_{12}EO_4$ with 12.5 (a) and 17 wt% APTES (b) at 25 ℃.

unordered lamellar structure changes to more ordered structure which induces the environment of ^{2}H nucleus transforms to the more anisotropic state, exhibiting a splitting double peaks (Figure 5c). For the two samples with high $C_{12}EO_4$ concentration, 40 wt% and 50 wt%, the more complicated spectra imply the formation of new self-assembly structures (Figure 5d and e). The single peak and the splitting shoulder peaks indicate the structure with multiple orientation which results in the anisotropic rotation of D_2O molecules. From the FF-TEM images in Figure 6 one can see that the lamellar structures outstretch in different orientations. Moreover, the decrease of the lamellar spacing with an increase of $C_{12}EO_4$ concentration

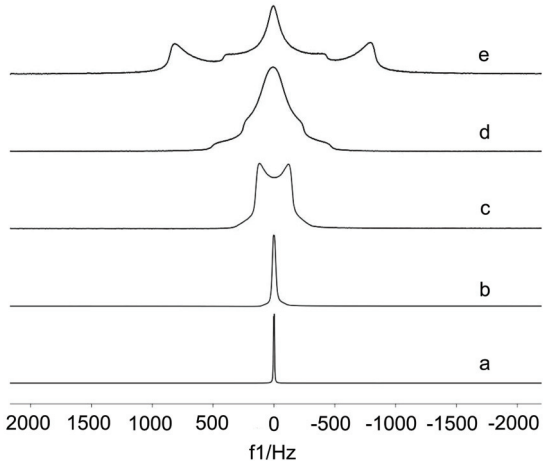

Figure 5 ^{2}H NMR spectra of samples formed by 5 wt% APTES with 10 (a), 20 (b), 30 (c), 40 (d), and 50 wt% $C_{12}EO_4$ (e) at 25 ℃.

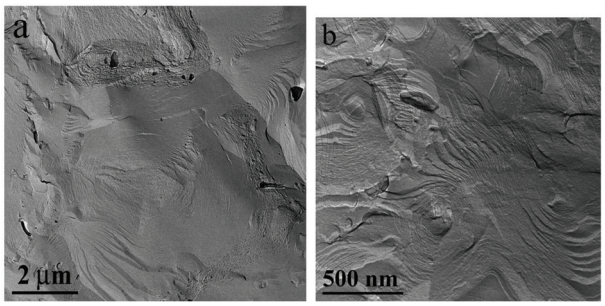

Figure 6 FF-TEM images of samples formed by 5 wt% APTES with 40 (a) and 50 wt% $C_{12}EO_4$ (b) at 25 ℃.

(shown in SAXS results) also slows the anisotropic rotation which induces the occurrence of the splitting in ^{2}H NMR determination.

3.3 SAXS measurements

Figures 7 and 8 provide SAXS information on the selected samples. From the position of the scattering peak (q), the lamellar spacing, d, which refers to the thickness of bilayer membrane and water layer, can be determined from $d=2\pi/q$.[28,29] For the four samples in the Line "EF", only one scattering peak was obtained for each sample (Figure 7) with the calculated lamellar spacing, d=19.76, 20.01,

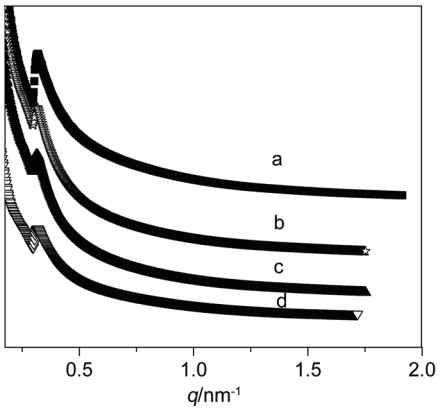

Figure 7 SAXS spectra of samples formed by 10 wt% $C_{12}EO_4$ with 10 (a), 12.5 (b), 15 (c), and 17 wt% APTES (d) at 25 ℃.

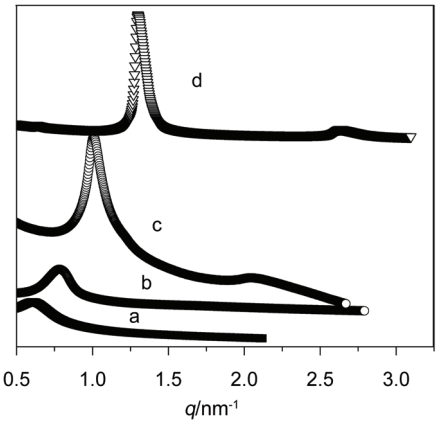

Figure 8 SAXS spectra of the lamellar structure formed by 5 wt% APTES with 20 (a), 30 (b), 40 (c), and 50 wt% $C_{12}EO_4$ (d).

20.01 and 19.70 nm, respectively, implying that the content of APTES makes less effect on lamellar spacing. The probable reason may be ascribed to the existence of APTES in the palisade of the bilayer membrane. For samples in the Line "MN", as shown in Figure 8, when $C_{12}EO_4$ concentration is below 30 wt%, only one scattering peak appears. From $q=0.606$ nm^{-1} and 0.782 nm^{-1} for the samples of 5 wt% APTES with 20 and 30 wt% $C_{12}EO_4$, the lamellar spacing d values are calculated to be 10.37 nm and 8.03 nm, respectively. For the samples of 40 wt% and 50 wt% $C_{12}EO_4$, two obvious scattering peaks with q_1 : q_2 being 1 : 2 were detected ($q=1.009$, 2.039 nm^{-1} at 40 wt% (curve c) and $q=1.304$, 2.639 nm^{-1} at 50 wt% (curve d)), which indicates the lamellar structure. The interlamellar spacings d for the two samples are 6.23 nm and 4.82 nm, respectively. From the above results, we can conclude that with an increase of $C_{12}EO_4$ concentration, the interlamellar spacing decreases continuously. The reason might be attributed to the extrusion of water molecules between the bilayers, which induces a denser packing of the bilayer membranes, as reported before.[30,31]

3.4 Rheological properties

Figures 9 and 10 show the oscillatory rheological properties of the samples formed by 10% $C_{12}EO_4$ with different APTES concentrations. When APTES concentration is lower than 15 wt%, the samples exhibit obvious viscoelasticity with an elasticity dominant property. The storage modulus (G') is one order magnitude greater than the loss storage (G''), both G' and G'' are almost independent of the frequency.[24] At higher APTES concentration, *e.g.*, 17 wt%, as is shown in Figure 9b, the viscoelasticity

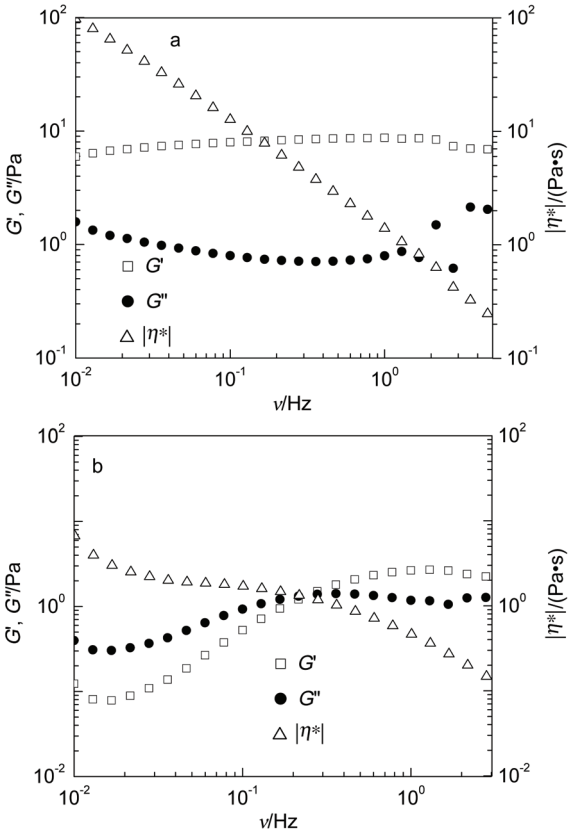

Figure 9 Oscillatory shear data of samples formed by 10% $C_{12}EO_4$ with 5 wt% (a) and 17 wt% APTES (b).

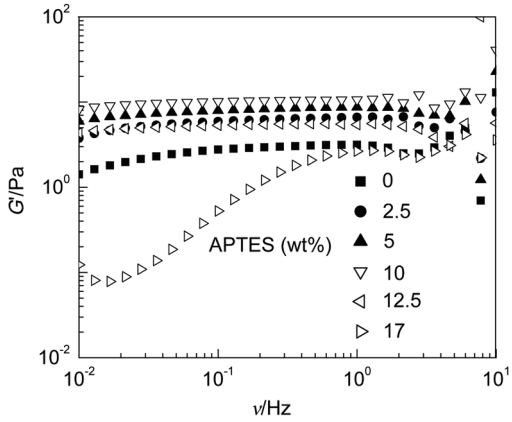

Figure 10 The elastic modulus (G') as a function of the oscillatory frequency for the samples formed by 10 wt% $C_{12}EO_4$ with different APTES concentrations.

decreases sharply with the oscillatory frequency. From Figure 10 one can also find that, with an increase of APTES content, the elasticity increases firstly, reaching a maximum value at about 10 wt%, and then decreases. The decrease of the viscoelasticity reflects the variation of the microstructures from vesicles to planar lamellar structures.

The rheological data of samples formed by 5 wt% APTES with different $C_{12}EO_4$ concentrations (10 wt%～50 wt%) are shown in Figures 11 and 12. For all selected samples, G' and G'' exhibit the frequency independent

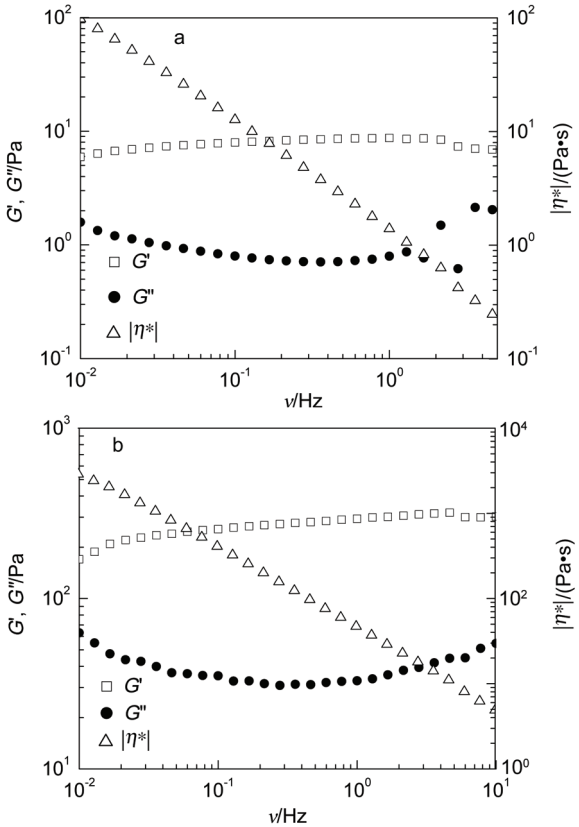

Figure 11 Oscillatory rheograms of the samples formed by 5 wt% APTES with 10 wt% (a) and 50 wt% $C_{12}EO_4$ (b).

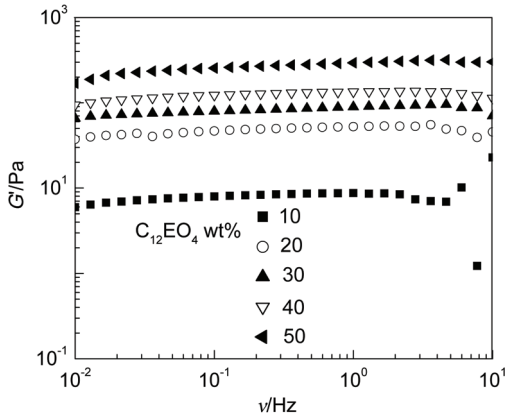

Figure 12 The elastic modulus (*G*') as a function of oscillatory frenquency for the samples formed by 5 wt% APTES with different $C_{12}EO_4$ concentrations at 25 ℃.

property and *G*' is about one order of magnitude higher than *G*", demonstrating the gel-like property (Figure 11). Figure 12 shows that, with an increase of $C_{12}EO_4$ concentration, *G*' also increases. Moreover, the samples also possess the gel-like appearance when $C_{12}EO_4$ concentration reaches 30 wt%. This is possibly caused by the formation of densely packed multi-lamellar vesicles (Figure 6).

Figure 13 shows the variation of shear viscosity and shear stress with an increase of the shear rate. All samples exhibit shear thinning behavior and the viscosity increases with an increase of $C_{12}EO_4$ concentration. For the samples

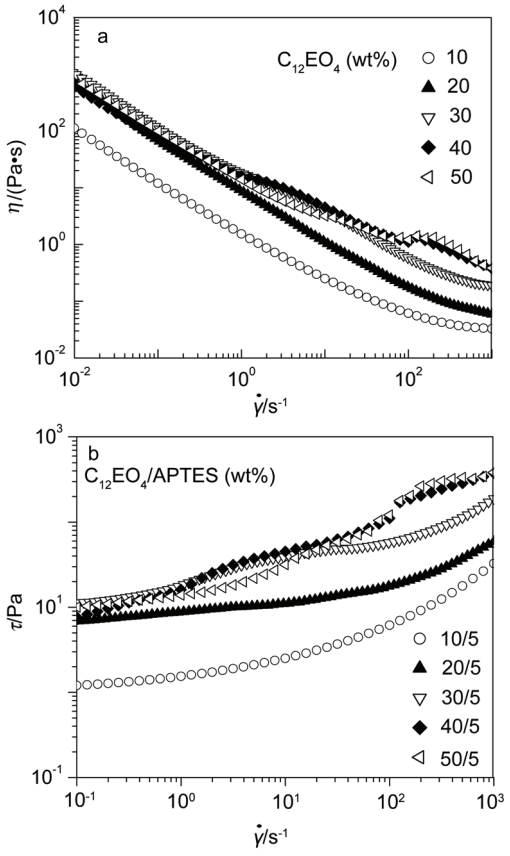

Figure 13 Shear viscosity (a) and shear stress (b) versus shear rate for samples of 5% APTES with different $C_{12}EO_4$ concentrations.

of 40 wt% and 50 wt% $C_{12}EO_4$, a partial shear thickening behavior is observed within the shear rate region of 60～100 s^{-1}. From Figure 13b the existence of yield stress can be observed for all samples with $C_{12}EO_4$ above 30%. It has been reported that the crowded population are multi-lamellar vesicles of the studied system, for which the outer layers can be peeled off under the shearing forces, producing more small vesicles, and results in the increase of the vesicle density.[24] Moreover, the shear can also induce the planar lamellar structures close to vesicles.[32~34] Due to the densely packed vesicles, the bilayers repel each other and the vesicles can not pass each other without deformation, which induces the high viscoelasticity and yield stress.

4 Conclusions

In conclusion, we report the phase behavior, self-assembly, and the rheological properties of $C_{12}EO_4$/APTES/H_2O system. With the variation of the composition, rich aggregation behavior can be obtained. The transition of aggregate structures from vesicle with higher curvatures to planar lamellar structure with low curvatures at the addition of APTES to $C_{12}EO_4$ aqueous solution was observed with a decrease of viscoelasticity. At a fixed APTES concentration, when $C_{12}EO_4$ concentration increases, a transition from vesicle to the co-existence of vesicles and planar lamellae occurs. Considering the wide use of silicon materials in the industry and material science, we hope our results can provide a guidance in the preparation of correlative materials.

References

[1] Dong, R.; Hao, J. *Chem. Rev.* **2010**, *110*, 4978.
[2] Gräbner, D.; Li, X.; Hoffmann, H.; Drechsler, M.; Schneider, O. *J. Colloid Interface Sci.* **2010**, *350*, 516.
[3] Seddon, J. M.; Raimondi, M. E. *Mol. Cryst. Liq. Cryst.* **2000**, *347*, 221.
[4] Albayrak, C.; Soylu, A. I. M.; Dag, Ö. *J. Colloid Interface Sci.* **2010**, *341*, 109.
[5] Fujimatsu, H.; Ogasawara, S.; Kuroiwa, S. *Colloid Polym. Sci.* **1988**, *266*, 594.
[6] Acharya, D. P.; Sato, T.; Kaneko, M.; Singh, Y.; Kunieda, H. *J. Phys. Chem. B* **2006**, *110*, 754.
[7] Rebbin, V.; Rothkirch, A.; Ohta, N.; Funari, S. S. *Langmuir* **2010**, *26*, 9017.
[8] Mitchell, D. J.; Tiddy, G. J. T.; Waring, L.; Bostock, T.; McDonald, M. P. *J. Chem. Soc., Faraday Trans.* **1983**, *79*, 975.
[9] Han, L.; Ye, Z.; Chen, H.; Luo, Y. *Acta Phys. Chim. Sin.* **2012**, *28*, 1405. (韩利娟, 叶仲斌, 陈洪, 罗平亚, 物理化学学报, **2012**, *28*, 1405.)
[10] Yuan, Z.; Yuan, J.; Lu, X.; Zhang, J.; Xu, G. *Acta Phys. Chim. Sin.* **2013**, *29*, 449. (苑再武, 苑敬, 吕鑫, 张健, 徐桂英, 物理化学学报, **2013**, *29*, 449.)
[11] Yue, H.; Guo, P.; Guo, R. *J. Chem. Eng. Data* **2009**, *54*, 2923.
[12] Dong, R.; Zhong, Z.; Hao, J. *Soft Matter* **2012**, *8*, 7812.
[13] Shao, Y.; Ma, Y. *Acta Chim. Sinica* **2012**, *70*, 1957. (邵悦, 马勇, 化学学报, **2012**, *70*, 1957.)
[14] Lei, J.; Yu, C.; Fan, J.; Yan, Y.; Tu, B.; Zhao, D. *Acta Chim. Sinica* **2005**, *63*, 739. (雷杰, 余承忠, 范杰, 闫妍, 屠波, 赵东元, 化学学报, **2005**, *63*, 739.)
[15] Kozerski, G. E.; Gallavan, R. H.; Ziemelis, M. J. *Anal. Chim. Acta* **2003**, *489*, 103.
[16] Rodriguez-Abreu, C.; Izawa, T.; Aramaki, K.; Lopez-Quintela, A.; Sakamoto, K.; Kunieda, H. *J. Phys. Chem. B* **2004**, *108*, 20083.
[17] Bryskhe, K.; Bulut, S.; Olsson, U. *J. Phys. Chem. B* **2005**, *109*, 9265.

[18] Olsson, U.; Nakamura, K.; Kunieda, H.; Strey, R. *Langmuir* **1996**, *12*, 3045.
[19] Khan, A.; Fontell, K.; Lindblom, G.; Lindman, B. *J. Phys. Chem.* **1982**, *86*, 4266.
[20] Jokela, P.; Jonsson, B.; Khan, A. *J. Phys. Chem.* **1987**, *91*, 3291.
[21] Coppola, L.; Gentile, L.; Nicotera, I.; Rossi, C. O.; Ranieri, G. A. *Langmuir* **2010**, *26*, 19060.
[22] Ge, L.; Guo, R.; Zhang, X. *J. Phys. Chem. B* **2009**, *113*, 1993.
[23] Medronho, B.; Shafaei, S.; Szopko, R.; Miguel, M. G.; Olsson, U.; Schmidt, C. *Langmuir* **2008**, *24*, 6480.
[24] Liu, C.; Hao, J.; Wu, Z. *J. Phys. Chem. B* **2010**, *114*, 9795.
[25] Medronho, B.; Schmidt, C.; Olsson, U.; Miguel, M. G. *Langmuir* **2010**, *26*, 1477.
[26] Lukaschek, M.; Müller, S.; Hasenhindl, A.; Grabowski, D. A.; Schmidt, C. *Colloid Polym. Sci.* **1996**, *274*, 1.
[27] Medronho, B.; Rodrigues, M.; Miguel, M. G.; Olsson, U.; Schmidt, C. *Langmuir* **2010**, *26*, 11304.
[28] Jiang, W.; Hao, J.; Wu, Z. *Langmuir* **2008**, *24*, 3150.
[29] Li, H.; Wieczorek, S. A.; Xin, X.; Kalwarczyk, T.; Ziebacz, N.; Szymborski, T.; Hołyst, R.; Hao, J.; Gorecka, E.; Pociecha, D. *Langmuir* **2010**, *26*, 34.
[30] Söderman, O.; Arvidson, G.; Lindblom, G.; Fontell, K. *Eur. J. Biochem.* **1983**, *134*, 309.
[31] Nettesheim, F.; Zipfel, J.; Lindner, P.; Richtering, W. *Colloids Surf. A* **2001**, *183～185*, 563.
[32] Regev, O.; Guillemet, F. *Langmuir* **1999**, *15*, 4357.
[33] Liu, J.; Han, W.; Zhang, Y.; Yao, C. *Acta Phys.-Chim. Sin.* **2010**, *26*, 1552. (刘金彦, 韩外慧, 张燕, 姚超怀, 物理化学学报, **2010**, *26*, 1552.)
[34] Liu, C.; Hao, J. *J. Phys. Chem. B* **2011**, *115*, 980.

(Cheng, F.)

